Supporting Information

Synergistic Effect of Lewis Acid-Base and Coulombic Interactions for High-performance Zn-I_2 Batteries

Jiafeng He,[a,b,†] Yongbiao Mu,[a,b,†] Buke Wu,[a,b] Fuhai Wu,[a,b] Ruixi Liao,[a,b] Hongfei Li,[c] Tianshou Zhao,[a,b*] and Lin Zeng[a,b*]

[a] *Shenzhen Key Laboratory of Advanced Energy Storage, Southern University of Science and Technology, Shenzhen 518055, P. R. China*

[b] *Department of Mechanical and Energy Engineering, Southern University of Science and Technology, Shenzhen 518055, P. R. China*

[c] *School of System Design and Intelligent Manufacturing, Southern University of Science and Technology, Shenzhen, 518055, P. R. China*

*E-mail: zhaots@sustech.edu.cn; zengl3@sustech.edu.cn

Experimental section

Preparation of ZIF-90. In a typical synthesis, a solid mixture of 0.296 g (1.00 mmol) zinc nitrate hexahydrate, 0.384 g (4.00 mmol) imidazole-2-formaldehyde, and 0.068 g (1.00 mmol) sodium formate was dissolved in 40 mL methanol by ultrasonic treatment. The as-prepared solution was placed in a Teflon-lined stainless steel autoclave, and heated at 85 ºC in an air-circulating oven for 24 h. After solvothermal reaction and cooling to 20 ºC, the ZIF-90 crystals were filtered and washed with methanol three times and then dried in air for 24 h at room temperature.

Preparation of IL-ZIF-90. To synthesize IL-ZIF-90 crystals, 0.35 g of dried ZIF-90 crystals and 1 g 1-aminopyridinium iodide (AmPyI) were suspended in 25 mL methanol and refluxed for 24 h at 50 °C. The reaction mixture was filtered, and the solid was washed with fresh methanol 2–3 times. The solid was further exchanged with fresh methanol for 24 h at 50 °C. The solid was dried for 24 h at 85 °C.

Preparation of IL-ZIF-90-I^-. First, the as-contained IL-ZIF-90 was mixed with Ketjen black and polyvinylidene fluoride binder in N-Methylpyrrolidone (NMP, Aladdin, AR) solvent on a mass ratio of 7:2:1, followed by vigorously stirring for 4 h. The slurry was then coated with the graphite paper substrate and dried at 60 ºC for 12 h to obtain a pristine IL-ZIF-90 electrode. After that, the electrode was immersed directly in 1 M ZnI_2 solution away from light for 12 h. Subsequently, the excess ZnI_2 solution was removed by dust-free paper and dried at 50 ºC under vacuum conditions for 12 h, protected from light, and finally, the IL-ZIF-90-I^- electrode was obtained. The ZIF-90-I^- electrode was prepared via the same procedure. The mass loading of I^- was around 2.0-2.5 mg cm^{-2} for IL-ZIF-90-I^- electrode, while the mass loading of I^- in ZIF-90-I^- electrode was 1.5-2.2 mg cm^{-2}.

Materials Characterization

The morphologies were characterized by Hitachi SU-8230 field emission scanning electron microscopy (FESEM, Hitachi SU-8230). Transmission electron microscopy (TEM), energy-dispersive X-ray analysis (EDX), and elemental mapping were

performed using a Talos instrument with an acceleration voltage of 300 kV. X-ray diffraction (XRD, Bruker Advance D8, Ultima IV with D/teX Ultra with Cu-Kα radiation) was employed to characterize the crystalline structures of samples with a scanning rate of 10° min^{-1}. X-ray photoelectron spectra (XPS, Escalab 250Xi) were acquired on a Thermo SCIENTIFIC ESCALAB 250Xi with Al Kα (hυ = 1486.8 eV) as the excitation source. UV-vis absorption spectra were collected by measuring the reacted electrolyte, which was obtained by dipping the electrode films and separators at different voltage states into the corresponding electrolytes, using a Lambda 365 UV-vis spectrophotometer (PerkinElmer) while employing the $ZnSO_4$ electrolyte as the reference. The specific surface area measurement was tested by a Specific surface and aperture analyzer (Micromeritics ASAP 2460). Flourier transformed Infrared (FTIR) spectroscopy was conducted on a Bruker VERTEX 70 & ALPHA spectrometer. To study the thermal stability of iodine, thermogravimetric was measured from 50 to 700 ℃ under an N_2 atmosphere with a heating rate of 10 ℃ min^{-1}, using a thermogravimetric analyzer (Discovery TGA).

Electrochemical measurements

CR2032 coin-type battery was assembled in the open-air environment using the as-above synthesized electrode as a cathode, glass fiber as the separator, 1 M $ZnSO_4$ solution as the aqueous electrolyte, and a zinc metal plate as the anode for electrochemical measurements. The electrochemical workstation (CHI 760D) was employed to record the cyclic voltammetry (CV) profiles and electrochemical impedance spectroscopy (EIS). Galvanostatic charge-discharge tests between 0.6 and 1.8 V versus Zn^{2+}/ Zn were performed on the LAND battery testing system and NETWARE battery analyzer.

Density functional theory calculation

All the density functional theory (DFT) calculations were carried out in the DMol3 package of Materials Studio 2018. The exchange-correlation potential was treated by using a generalized gradient approximation (GGA) with the Perdew-Burke-

Ernzerhof (PBE) parametrization. [1,2] A cutoff energy of 450 eV was set. The electronic energy was considered self-consistent when the energy change was smaller than 10^{-5} eV, while the tolerance convergence in ionic was also 10^{-5} eV. Furthermore, the van der Waals correction of Grimme's DFT-D3 model was adopted.[3-5] The different charge densities can be defined as $\Delta\rho=\rho_*(I^-/I_2/I_3^-)-\rho_*-\rho(I^-/I_2/I_3^-)$, where $\rho_*(I^-/I_2/I_3^-)$, ρ_*, and $\rho(I^-/I_2/I_3^-)$ are the electron densities of the IF-ZIF-90 with the adsorbed $I^-/I_2/I_3^-$ molecule, the IF-ZIF-90, and isolated $I^-/I_2/I_3^-$ molecule, respectively. The adsorption energy E_{ads} per $I^-/I_2/I_3^-$ molecule can be defined as, $E_{ads}=E^*(I^-/I_2/I_3^-)-E^*-E(I^-/I_2/I_3^-)$, where $E^*(I^-/I_2/I_3^-)$ stands for the energy of the IF-ZIF-90 with the adsorbed $I^-/I_2/I_3^-$ molecule, E* is the energy of IF-ZIF-90, and $E(I^-/I_2/I_3^-)$ is the energy of an $I^-/I_2/I_3^-$ molecule under vacuum.

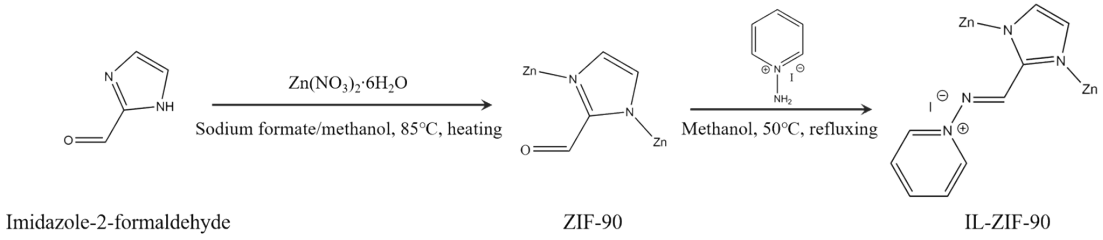

Figure S1. Synthesis routine of IL-ZIF-90.

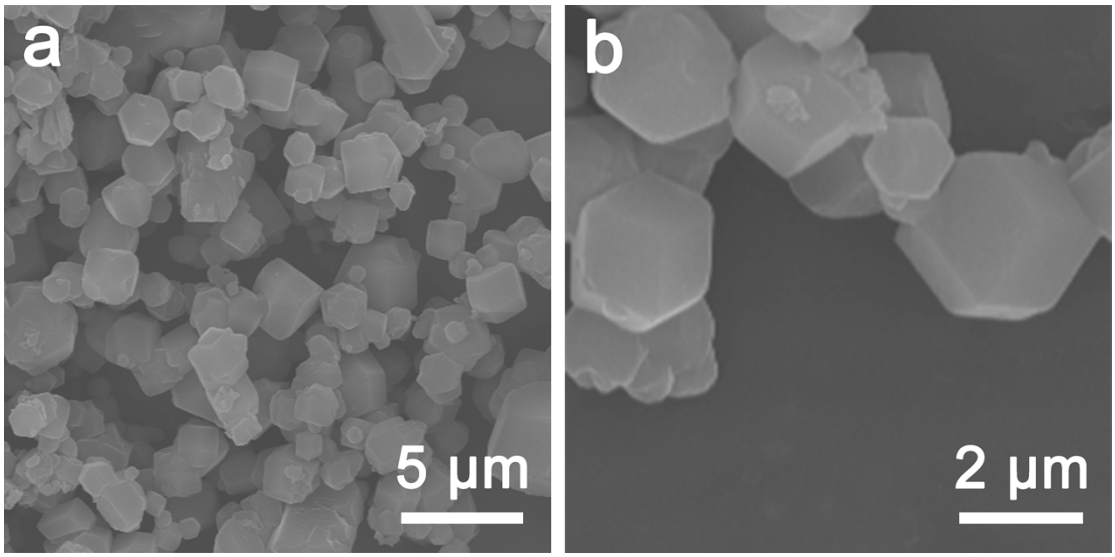

Figure S2. (a, b) FESEM images of ZIF-90 at different magnifications.

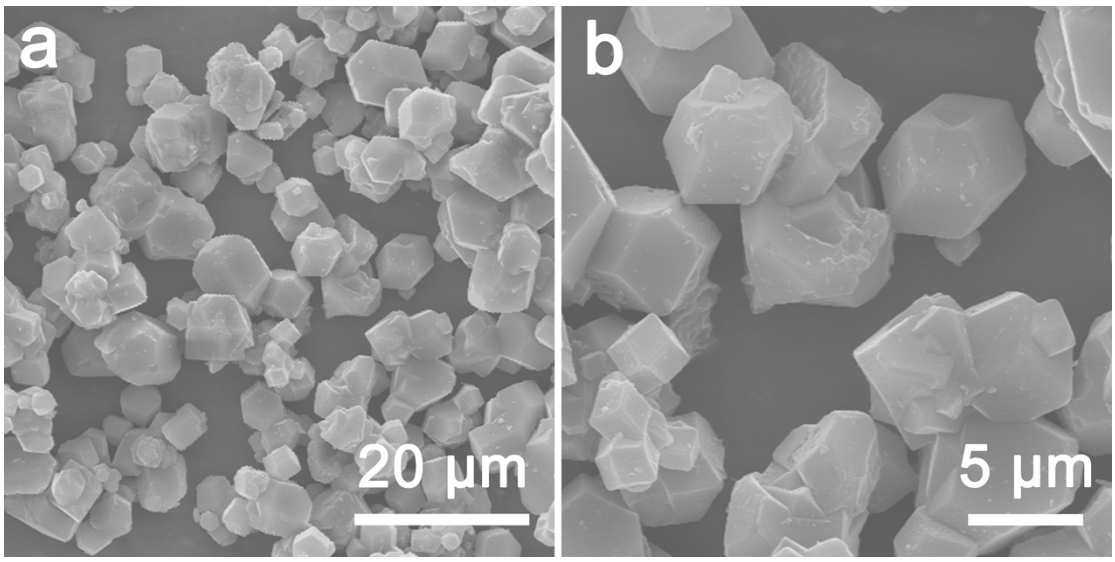

Figure S3. (a, b) FESEM images of IL-ZIF-90 at different magnifications.

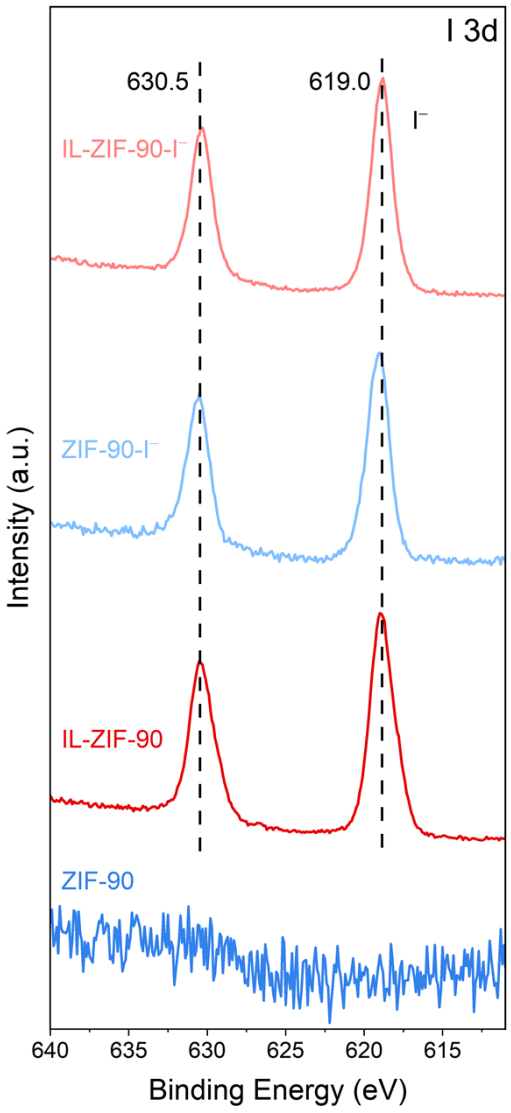

Figure S4. High-resolution XPS spectra of I 3d for ZIF-90, IL-ZIF-90, ZIF-90-I^- and IL-ZIF-90-I^-.

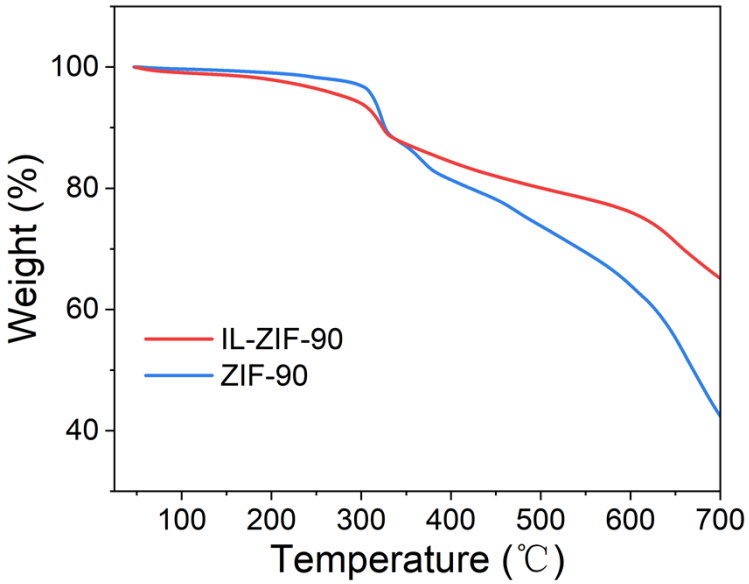

Figure S5. TGA curves of ZIF-90 and IL-ZIF-90

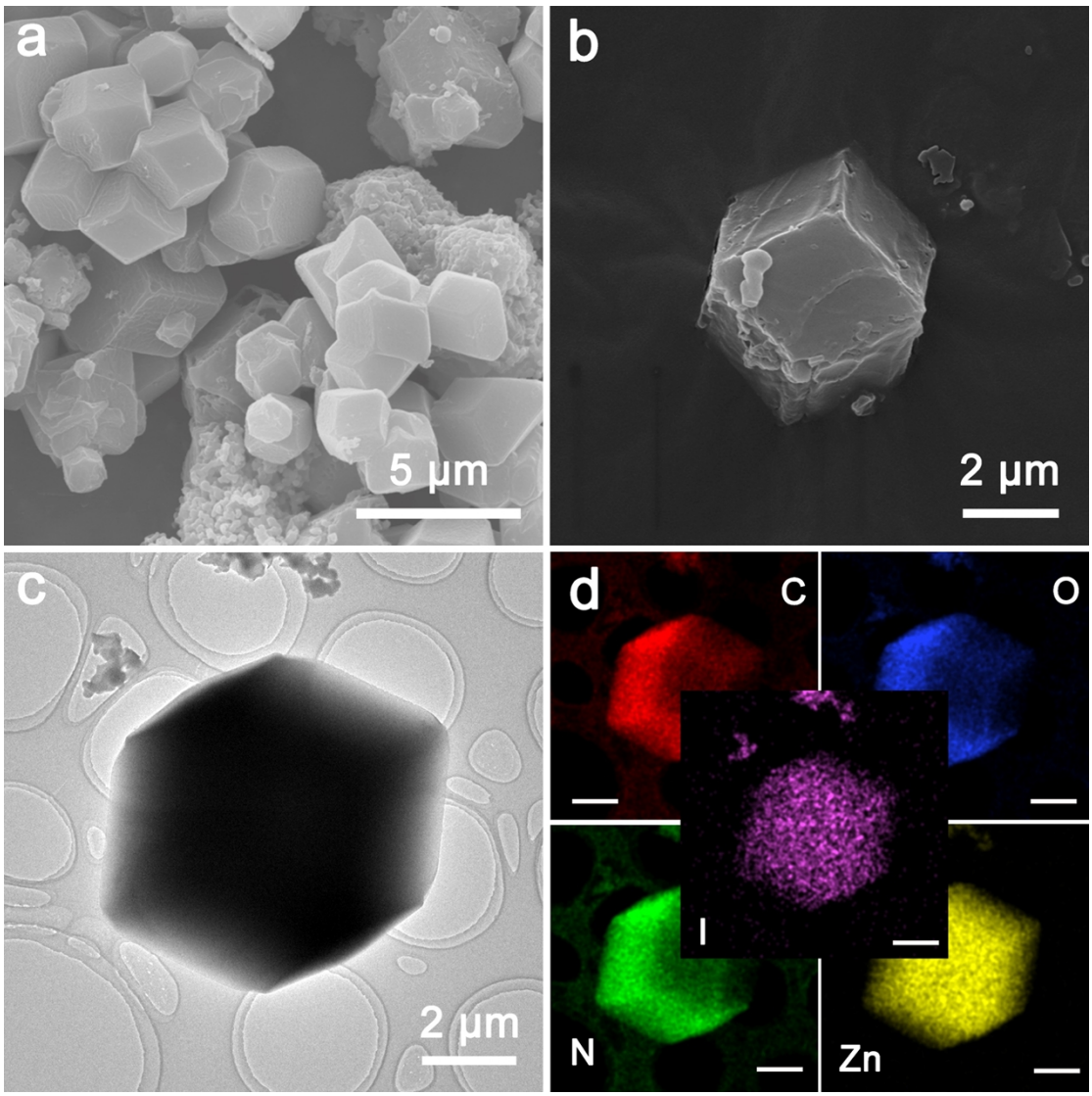

Figure S6. (a, b) FESEM images of ZIF-90-I^- at different magnifications. (c) TEM image of ZIF-90-I^-, and (d) corresponding EDS elemental mappings of C, O, N, Zn, and I.

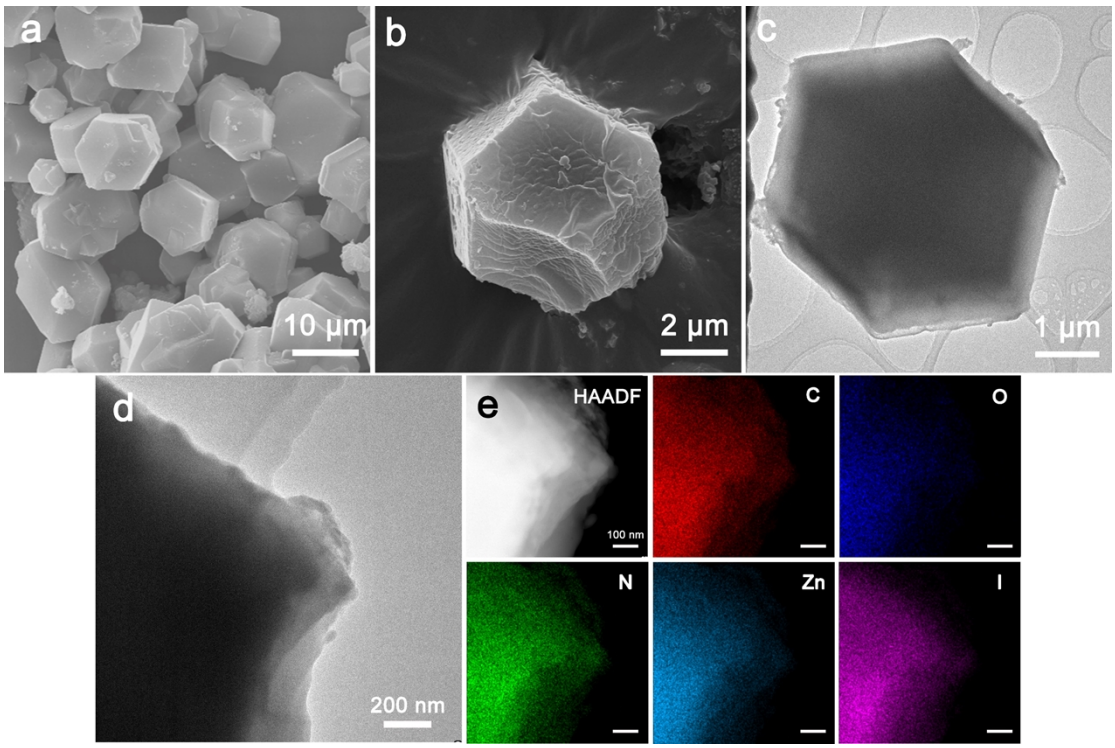

Figure S7. (a, b) FESEM images of IL-ZIF-90-I^- at different magnifications. (c) TEM and (d) HRTEM images of IL-ZIF-90-I^-. (e) HAADF-STEM image and corresponding EDS elemental mappings of C, O, N, Zn, and I.

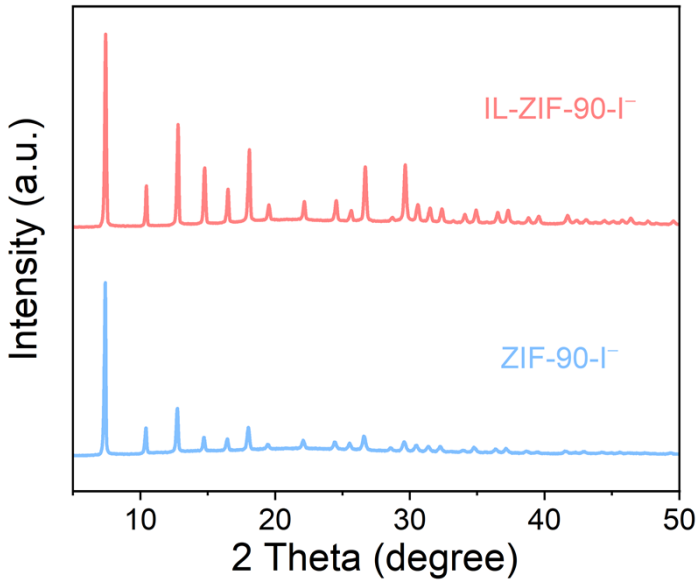

Figure S8. XRD patterns of ZIF-90-I⁻ and IL-ZIF-90-I⁻.

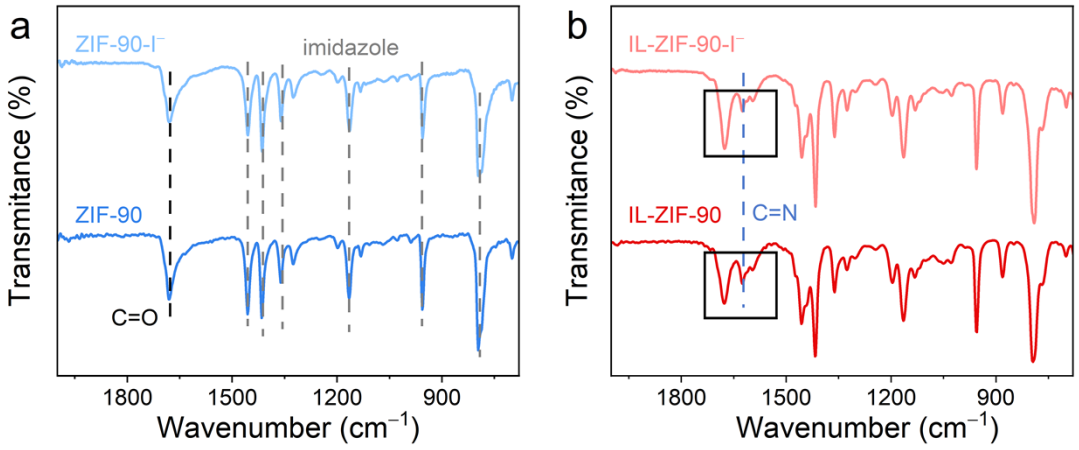

Figure S9. FTIR spectra of (a) ZIF-90 and (b) IL-ZIF-90 before and after adsorbing iodine.

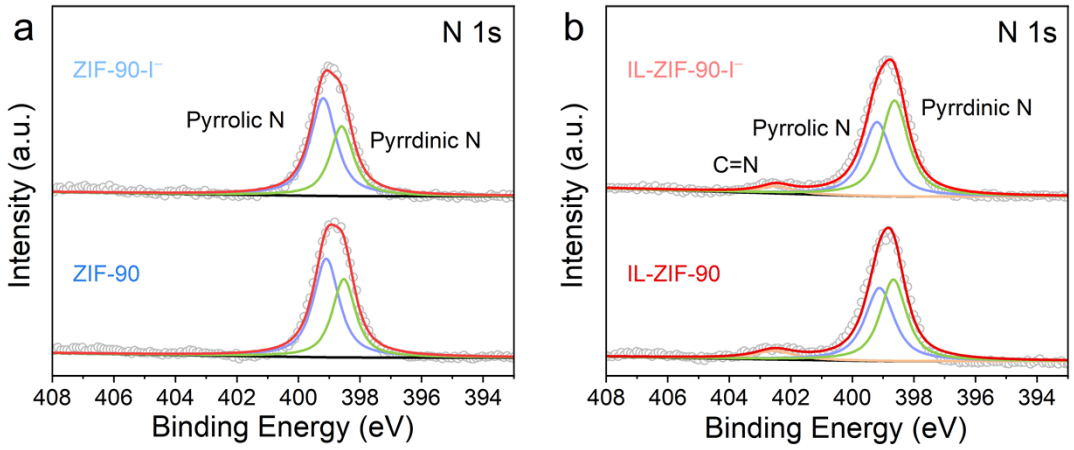

Figure S10. High-resolution XPS spectra of N 1s for (a) ZIF-90 and (b) IL-ZIF-90 before and after adsorbing iodine.

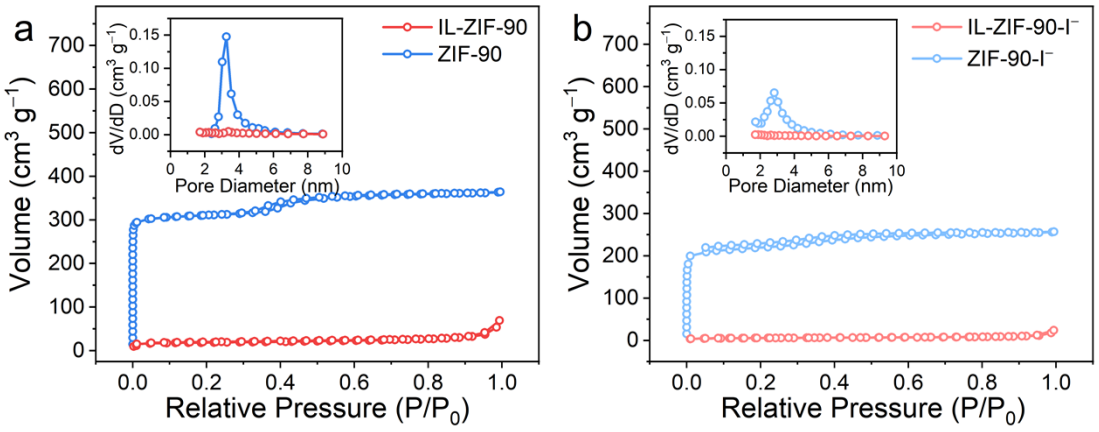

Figure S11. N_2 adsorption−desorption isotherms (inset shows corresponding micropore distributions) of ZIF-90 and IL-ZIF-90 (a) before and (b) after adsorbing iodine.

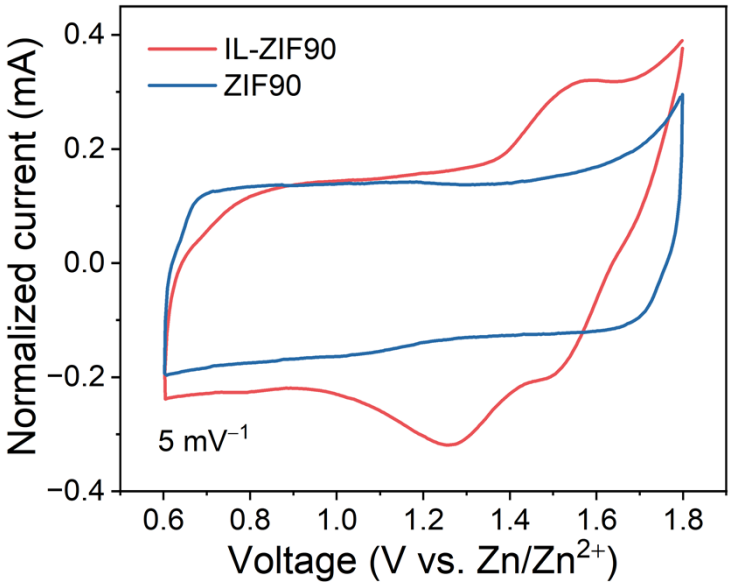

Figure S12. CV curves of ZIF-90 and IL-ZIF-90 electrodes at a scan rate of 5 mV s^{-1}.

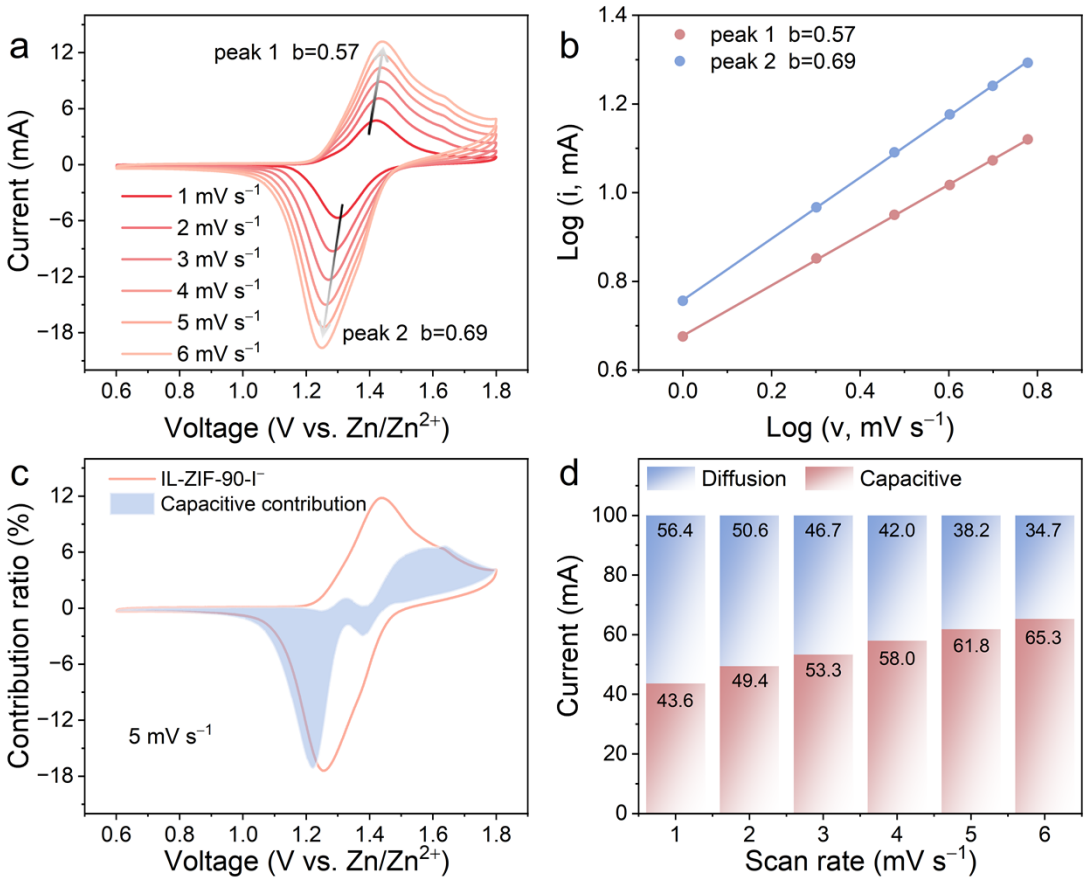

Figure S13. The reaction kinetics of IL-ZIF-90-I$^-$ cathode. (a) CV curves at different scan rates. (b) Log (*i*) vs. log (*v*) plots of the cathodic and anodic current responses at peaks shown in the CV curves. (c) The illustration of the calculated capacitive and diffusion-controlled contributions of IL-ZIF-90-I$^-$ cathode at 5 mV s^{-1}. (d) Contribution ratio of the capacitive- and diffusion-controlled process of IL-ZIF-90-I$^-$ cathode at various scan rates.

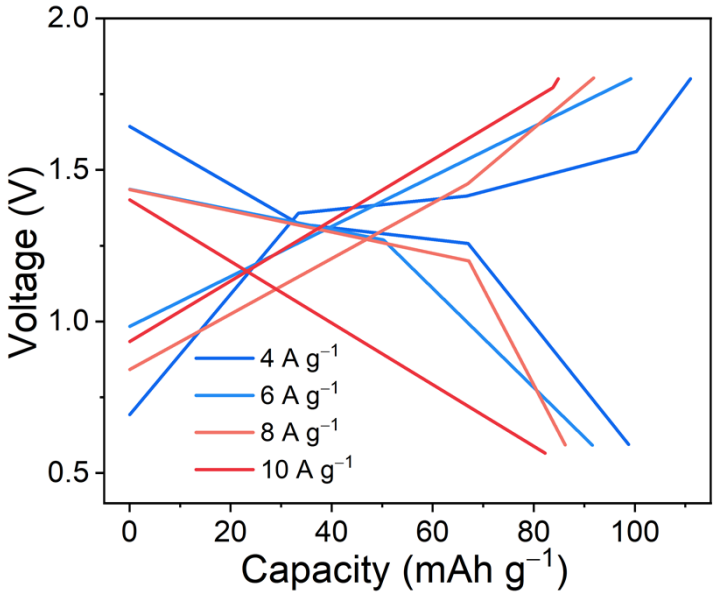

Figure S14. GCD curves of ZIF-90-I^- electrode at various rates.

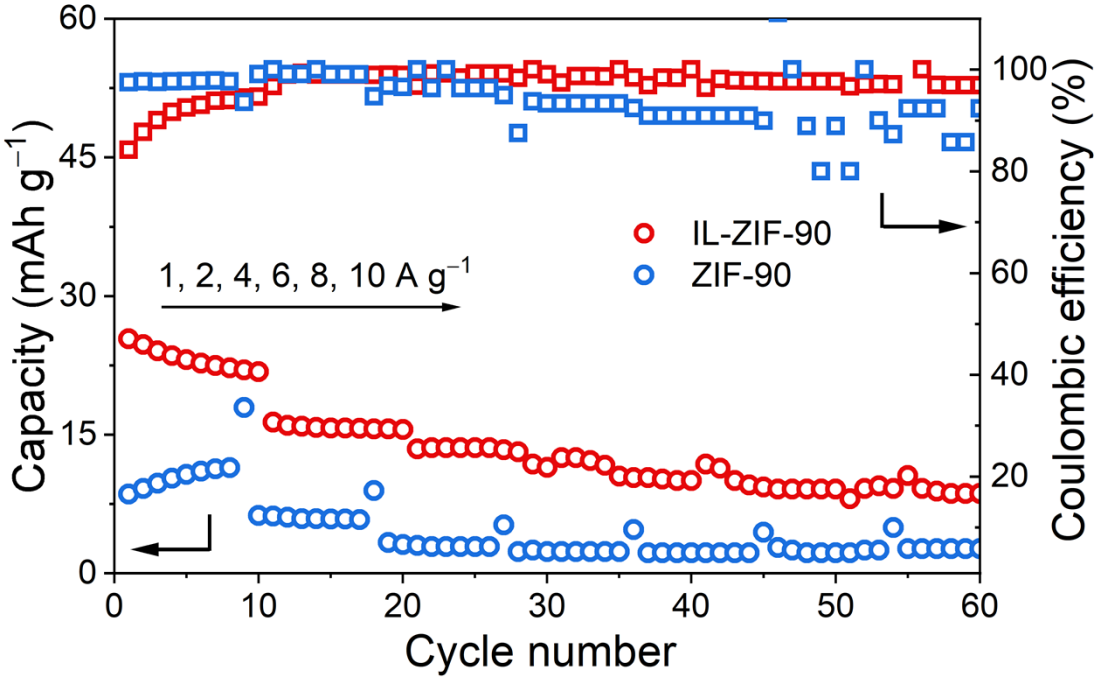

Figure S15. The rate capability of ZIF-90 and IL-ZIF-90 electrodes.

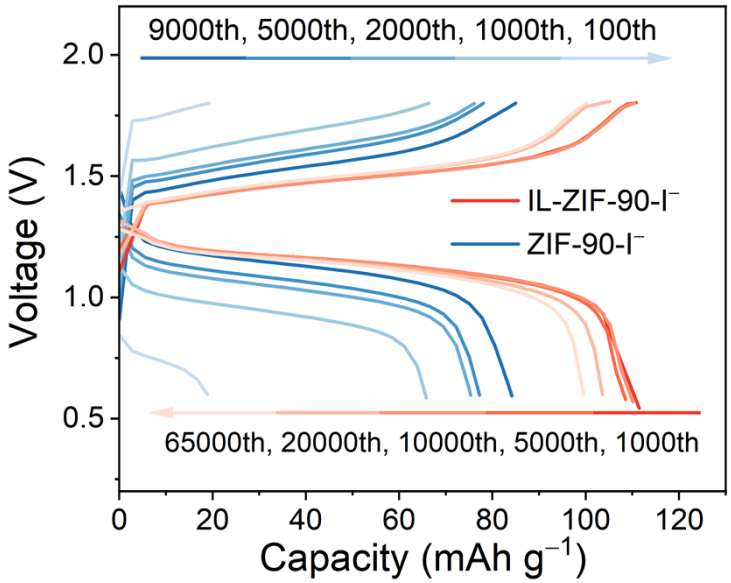

Figure S16. GCD curves of ZIF-90-I⁻ and IL-ZIF-90-I⁻ electrodes at 10 A g^{-1}.

Table S1. The cell performance comparison of zinc-iodine cells.

Materials	**Cycle number**	**Current density ($A\ g^{-1}$)**	**Capacity retention (%)**	**Ref.**
Zn-BTC membrane	6000	1.92	84.6	1
I_2–Nb_2CT_X MXene electrode	23000	6	80	2
SC-PPS@Zn	6000	3.2	90.2	3
Zeolite-Zn	5600	2	91.9	4
Zn-TCPP	5000	5	68.4	5
$Co[Co_{1/4}Fe_{3/4}(CN)_6]/I_2$	2000	4	80.2	6
Zn@ZSO	10000	2	66.7	7
$ODAI_2$	10000	4.5	80	8
IL-ZIF-90-I^-	65000	10	91.7	This work

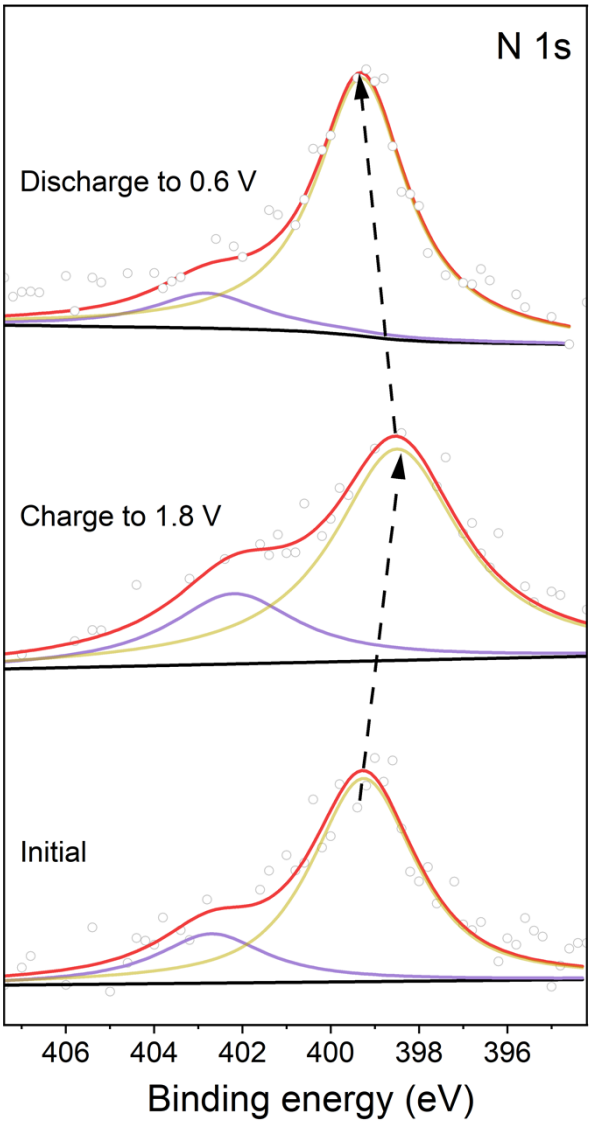

Figure S17. High-resolution XPS spectra of N 1s for IL-ZIF-90-I^- electrode at various states.

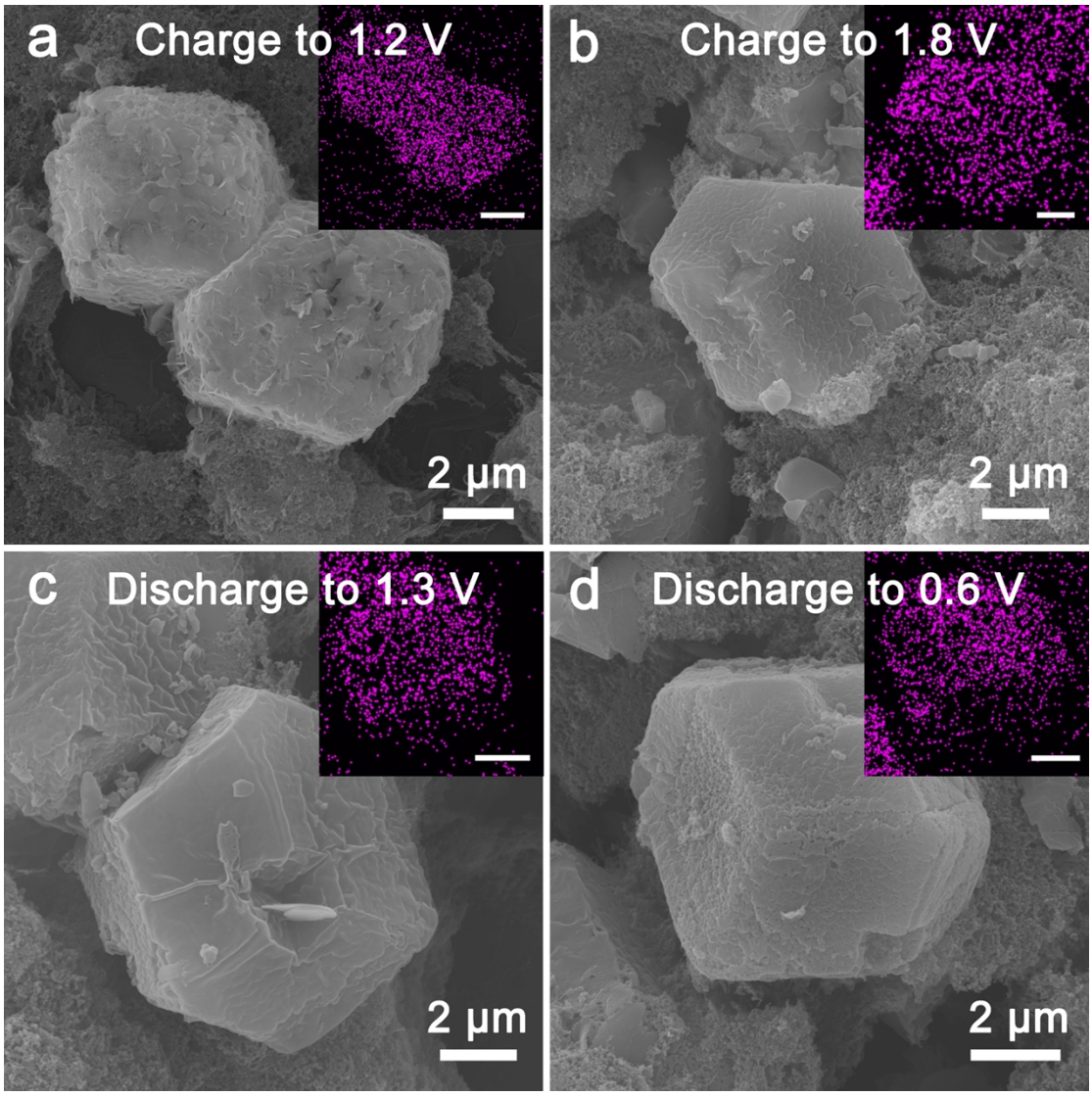

Figure S18. SEM images with the iodine element mapping of IL-ZIF-90-I^- cathodes at different electrochemical states: (a) charge to 1.2 V, (b) charge to 1.8 V, (c) discharge to 1.3 V, (d) discharge to 0.6 V.

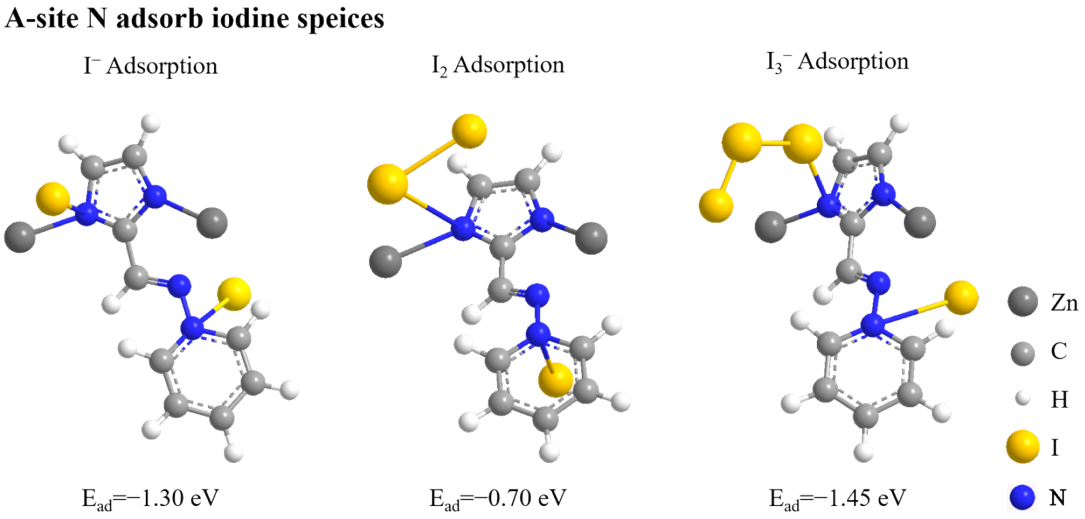

Figure S19. The proposed adsorption model of A-site N for iodine species and calculated adsorption energies.

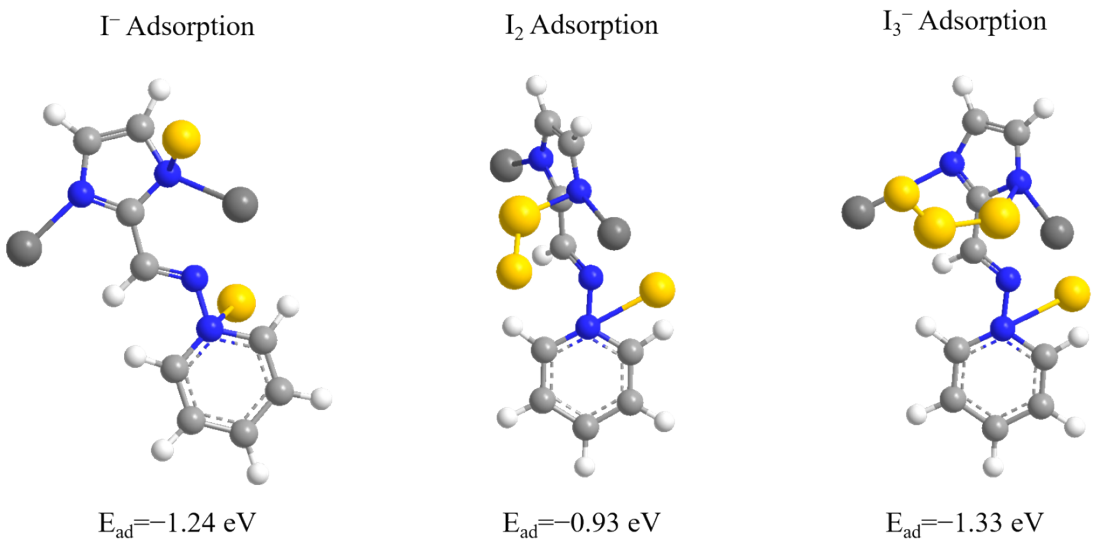

Figure S20. The proposed adsorption model of B-site N for iodine species and calculated adsorption energies.

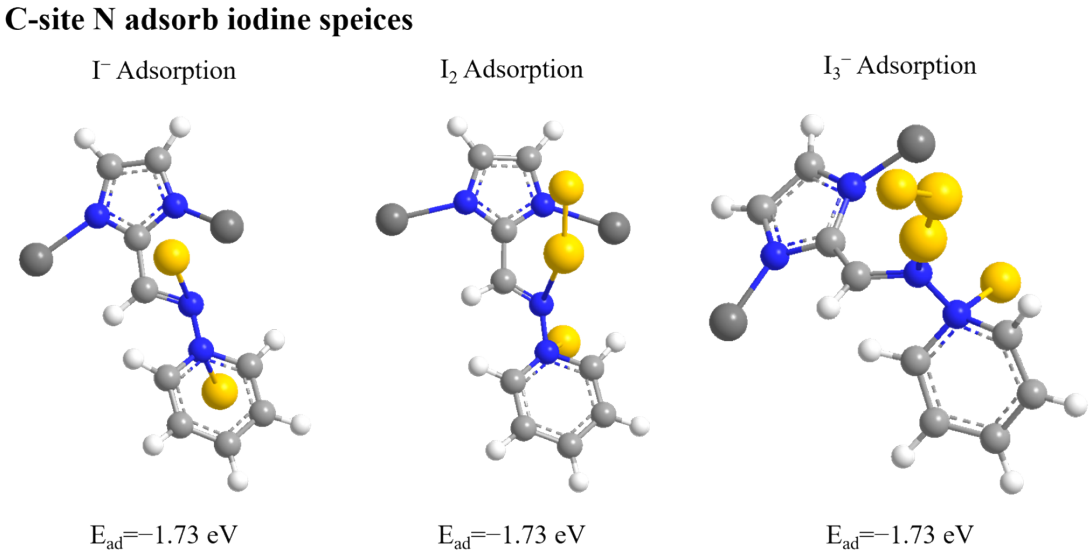

Figure S21. The proposed adsorption model of C-site N for iodine species and calculated adsorption energies.

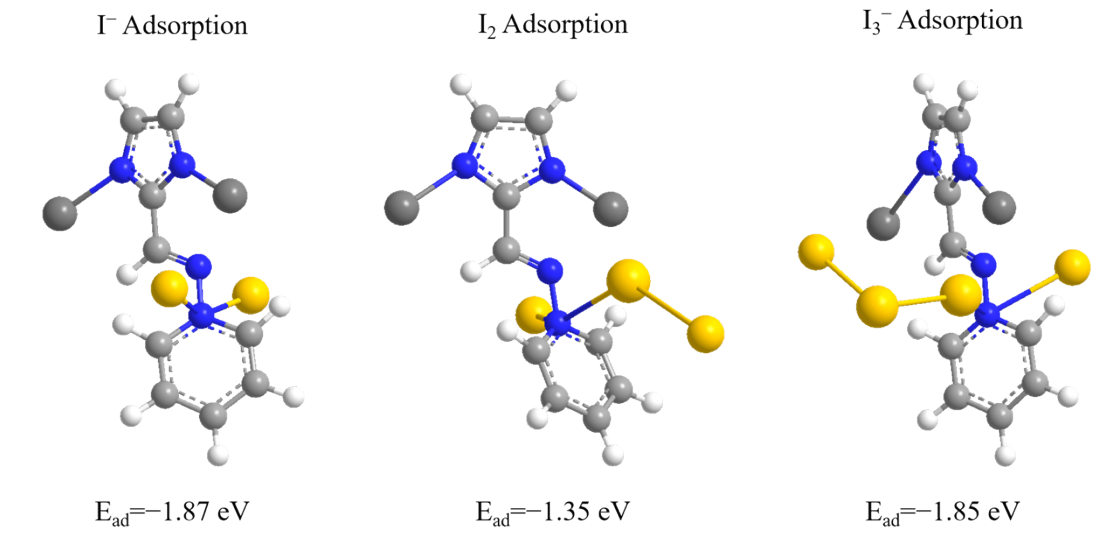

Figure S22. The proposed adsorption model of D-site N for iodine species and calculated adsorption energies.

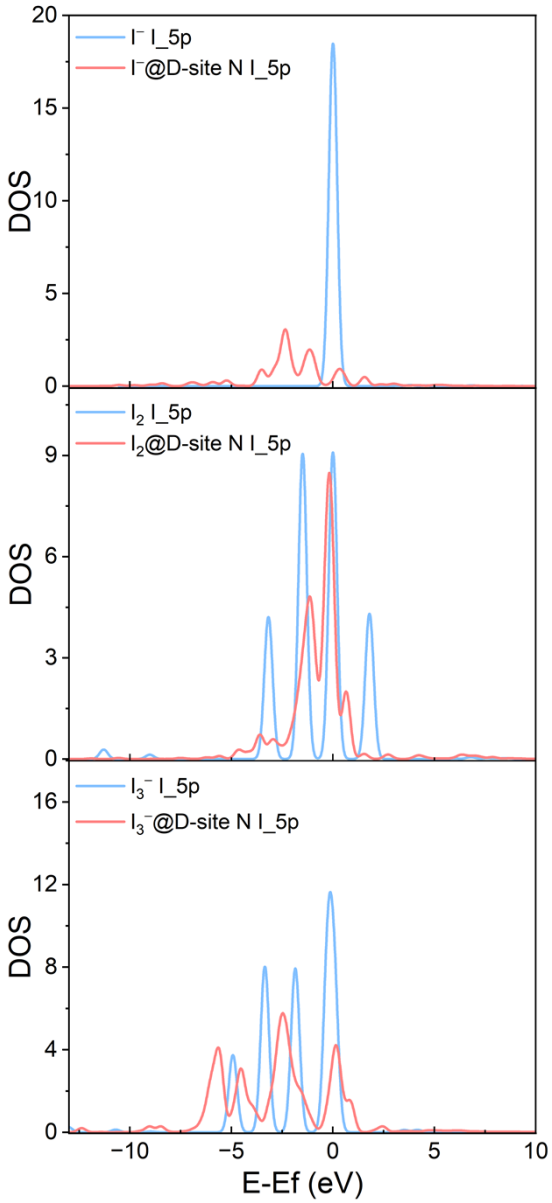

Figure S23. Partial density of the states (PDOS) for I 5p orbital of various iodine species (I^-, I_2, and I_3^-) before and after adsorption on D-site N.

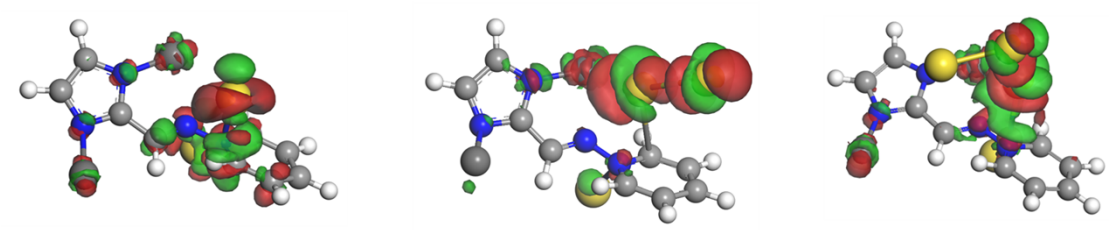

Figure S24. Optimized charge-density-difference patterns of I^-, I_2, and I_3^- on D-site N.

References

[1] H. Yang, Y. Qiao, Z. Chang, H. Deng, P. He and H. Zhou, *Adv. Mater.*, 2020, **32**, 2004240.

[2] X. Li, N. Li, Z. Huang, Z. Chen, G. Liang, Q. Yang, M. Li, Y. Zhao, L. Ma, B. Dong, Q. Huang, J. Fan, C. Zhi, Adv. Mater. **2021**, 33, 2006897.

[3] L. Zhang, J. Huang, H. Guo, L. Ge, Z. Tian, M. Zhang, J. Wang, G. He, T. Liu, J. Hofkens, D. J. L. Brett and F. Lai, *Adv. Energy Mater.*, 2023, **13**, 2203790.

[4] W. Shang, Q. Li, F. Jiang, B. Huang, J. Song, S. Yun, X. Liu, H. Kimura, J. Liu and L. Kang, *Nanomicro Lett.*, 2022, **14**, 82.

[5] Y. Tan, Z. Chen, Z. Tao, A. Wang, S. Lai and Y. Yang, *Angew. Chem. Int. Ed.*, 2023, **62**, e202217744.

[6] L. Ma, Y. Ying, S. Chen, Z. Huang, X. Li, H. Huang and C. Zhi, *Angew. Chem. Int. Ed.*, 2021, **60**, 3791-3798.

[7] H. Peng, Y. Fang, J. Wang, P. Ruan, Y. Tang, B. Lu, X. Cao, S. Liang and J. Zhou, *Matter*, 2022, **5**, 4363-4378.

[8] X. Li, S. Wang, T. Wang, Z. Duan, Z. Huang, G. Liang, J. Fan, C. Yang, A. L. Rogach and C. Zhi, *Nano Energy*, 2022, **98**, 107278.